AGU PUBLICATIONS

JGR

Journal of Geophysical Research: Atmospheres

RESEARCH ARTICLE
10.1002/2014JD022534

Key Points:
- Single database is stratified into smaller and more homogeneous databases
- Results from stratified databases greatly outperform that from single database
- Including relative humidity and vertical velocity is beneficial for snow detection

Correspondence to:
Y. You,
yyou@umd.edu

Citation:
You, Y., N.-Y. Wang, and R. Ferraro (2015), A prototype precipitation retrieval algorithm over land using passive microwave observations stratified by surface condition and precipitation vertical structure, *J. Geophys. Res. Atmos.*, *120*, 5295–5315, doi:10.1002/2014JD022534.

Received 3 SEP 2014
Accepted 9 APR 2015
Accepted article online 15 APR 2015
Published online 1 JUN 2015

A prototype precipitation retrieval algorithm over land using passive microwave observations stratified by surface condition and precipitation vertical structure

Yalei You[1], Nai-Yu Wang[2], and Ralph Ferraro[3]

[1]Cooperative Institute for Climate and Satellite, University of Maryland, College Park, Maryland, USA, [2]IMSG, STAR, NESDIS, NOAA, College Park, Maryland, USA, [3]STAR, NESDIS, NOAA, College Park, Maryland, USA

Abstract A prototype precipitation retrieval algorithm over land has been developed by utilizing 4 year National Mosaic and Multi-Sensor Quantitative Precipitation Estimation and Special Sensor Microwave Imager/Sounder coincident data sets. One of the unique features of this algorithm is using the ancillary parameters (i.e., surface type, surface temperature, land elevation, and ice layer thickness) to stratify the single database into many smaller but more homogeneous databases, in which both the surface condition and precipitation vertical structure are similar. It is found that the probability of detection (POD) increases about 8% and 12% by using stratified databases for rainfall and snowfall detection, respectively. In addition, by considering the relative humidity at lower troposphere and the vertical velocity at 700 hPa in the precipitation detection process, the POD for snowfall detection is further increased by 20.4% from 56.0% to 76.4%. The better result is evident in both ends of the retrieved rain rate when the stratified databases are used, especially when the rain rate is greater than 30 mm/h. Similarly, the retrieved snowfall rate using stratified databases also outperforms that using single database. The correlation between retrieved and observed rain rates from stratified databases is 0.63, while it is 0.42 using the single database. The root-mean-square error is reduced by 50.3% from 2.07 to 0.98 by using stratified databases. The retrieved snow rates from stratified database are also better correlated with observations and possess smaller root-mean-square error. Additionally, the precipitation overestimation from the single database over the western United States is largely mitigated when the stratified databases are utilized. It is further demonstrated that over the majority of the stratified databases, the relationship between precipitation rate and brightness temperature is much closer to that from the corresponding category in the validation databases, rather than that from the single database. Therefore, overall superior performance using the stratified databases for both the precipitation detection and retrieval is achieved.

1. Introduction

Accurate measurement of precipitation is of critical importance for many applications ranging from short-term weather analysis and prediction to long-term climate monitoring. Satellite observations from microwave radiometers provide the opportunity to measure precipitation on the global scale. Numerous precipitation retrieval algorithms using satellite microwave observations have been developed over land in the past several decades.

In the early work, the rainfall rate over land is simply derived from the brightness temperature (TB) at high frequency (e.g., 85 GHz) without considering either cloud vertical structure or land surface condition. For example, *Spencer et al.* [1989] utilized the "polarization-corrected temperature" (PCT) to detect and retrieve rainfall over land. The PCT is almost identical to TB at 85 GHz over land. The "scattering index" (SI), which is calculated based on TB at 85 GHz, was initially proposed by *Grody* [1991] and later improved by *Ferraro et al.* [1994] and *Ferraro and Marks* [1995] to identify and retrieve rainfall over land. This method serves as the basis for Tropical Rainfall Measurement Mission facility rain retrieval algorithm over land. *Adler et al.* [1993] directly used the TB at 85 GHz to retrieve rainfall over land areas. *Liu and Curry* [1992] attempted to use both emission and scattering signature to retrieve rainfall. However, over land it is still the TB at high frequency that provides the majority of the rainfall information. These types of algorithms have difficulties to capture the precipitation signature when there exists no or little ice in the cloud systems.

It has long been recognized that stratiform and convective rainfall have much different vertical structures [e.g., *Berg et al.*, 2002; *Hirose and Nakamura*, 2004; *You and Liu*, 2012; *Wang et al.*, 2012; *Liu and Zipser*, 2013]. More sophisticated algorithms have been developed in recent years to incorporate the stratiform and convective information [*Aonashi et al.*, 2009; *Gopalan et al.*, 2010; *Kummerow et al.*, 2011; *Sano et al.*, 2013; *Petty and Li*, 2013]. A convective percentage index (CPI) was proposed by *McCollum and Ferraro* [2003]. By doing this, the final rain rate is calculated as a weighted average between convective and stratiform rain rates. An improved CPI has also been used by *Gopalan et al.* [2010] for the rainfall retrieval over land, where a more comprehensive data set was utilized. Storm top height estimated from TB has been used by *Aonashi et al.* [2009] to identify the deep convective rainfall. They found that severe overestimation without considering storm height is mitigated for tall precipitation cases. In *Sano et al.* [2013], several large-scale environmental parameters derived from reanalysis data were utilized to roughly separate the rainfall profiles in the predefined database from model simulations. It was shown that the retrieval results are improved greatly due to the reduced ambiguity in the database. Over ocean, *Kummerow et al.* [2011] utilized the total precipitable water to identify the shallow convective regions. The total precipitable water has also been utilized over land to identify the precipitation regimes in the most recent version of Goddard profiling algorithm (GPROF2014), according to the GPROF2014 Passive Microwave Algorithm Theoretical Basis Document, version 1.4 (http://rain.atmos.colostate.edu/ATBD/).

Another major obstacle for precipitation retrieval over land is the high and highly variable land surface emissivity. Unlike the emissivity over ocean, it is difficult to accurately calculate the emissivity over land, especially under raining conditions [e.g., *Prigent et al.*, 2006; *Wang et al.*, 2009; *Ferraro et al.*, 2013; *Turk et al.*, 2013; *You et al.*, 2013]. To take the emissivity influence into consideration, *Aonashi et al.* [2009] described a scheme in which the entire globe is divided into thousands of $5 \times 5°$ grid boxes for each season. Look-up tables are constructed for each grid box in each season. The land surface is divided into six different types based on the clear-sky TBs in *Petty and Li*'s [2013] work. In the GPROF2014 algorithm for the Global Precipitation Measurement (GPM) satellite, the land surface type information derived from the Tool to Estimate Land-Surface Emissivities at Microwave frequencies (TELSEM) [*Aires et al.*, 2011] has also been used. To avoid the surface emissivity effects, instead of using the signatures from window channels (e.g., 85GHz), *Staelin and Chen* [2000] introduced a different technique to estimate surface precipitation which depends solely on microwave observations near opaque water vapor and oxygen absorption channels (183 GHz and 52 GHz).

Commonly, the precipitation detection is performed for each new observation before the actual precipitation retrieval algorithm is applied. Most of the rainfall detection techniques [e.g., *Grody*, 1991; *Ferraro et al.*, 1994; *Adler et al.*, 1994; *Conner and Petty*, 1998; *Seto et al.*, 2005; *Kacimi et al.*, 2013] utilized the scattering index (SI) concept proposed by *Grody* [1991]. A comprehensive review of SI technique for rainfall detection can be found in *Seto et al.* [2005]. It is worth mentioning that in *Petty and Li*'s [2013] algorithm, no rain detection procedure is employed, and therefore, the retrieved rain rate for each new observation will always be a nonnegative value, no matter how small it is. It depends on the users to decide whether to treat a pixel as raining or nonraining based on the magnitude of the retrieved rain rate. Unlike rainfall detection, snowfall detection has a much shorter history and is still at a very early stage of development. Several snowfall detection techniques have been developed [e.g., *Kongoli et al.*, 2003; *Skofronick-Jackson et al.*, 2004; *Liu and Seo*, 2013], and it is generally agreed that TB at high frequencies (> 80 GHz) is capable of detecting the falling snow [e.g., *Katsumata et al.*, 2000; *Bennartz and Bauer*, 2003; *Skofronick-Jackson et al.*, 2013]. Recently, *Turk et al.* [2013] proposed a linear discriminant analysis (LDA) technique for rainfall detection. It was shown that the detection performance is superior to the traditional SI method, especially in the winter season. This technique will be adopted into our current work for both rainfall and snowfall detection, with some modifications (see section 3).

None of the aforementioned algorithms have taken both rain vertical structure and surface condition into consideration for detecting and estimating the surface precipitation from TBs. On the one hand, TB measured by a passive microwave radiometer reflects the integrated effects of ice and water paths, not surface rain rate; therefore, different TBs resulting from different rain vertical structures could very possibly correspond to similar surface rain rate [e.g., *Kummerow et al.*, 2011; *You and Liu*, 2012]. On the other hand, large retrieval uncertainties could also be caused by the different land surface backgrounds (e.g., dense vegetation versus bare ground) due to the large variation of the surface emissivities. Although the high-frequency channel (e.g., 85 GHz) is "blind" to the surface when the precipitation is heavy, the effect from the land surface is not negligible for the light precipitation, as shown by *You* [2013]. Further, previous work has shown that including low-frequency channels into the rainfall retrieval algorithm development could also be very beneficial.

For example, *Aonashi et al.* [2009] pointed out that by including the TB at 37 GHz in the retrieval process, it was found that severe overestimation is mitigated for deep precipitation systems. Two low-frequency channel combination contains both liquid and ice information, as shown by *You et al.* [2011]. To better use the low-frequency channels, the surface emissivity information is indispensable.

Therefore, the primary objective of this study is to develop a new precipitation retrieval algorithm by considering both land surface condition and precipitation vertical structure. Toward this end, several physical parameters will be used to stratify the single database into many smaller but more homogeneous databases for precipitation detection and retrieval. Our goal is to make sure both the surface condition and precipitation vertical structure are as homogeneous as possible in each stratified database. By doing this, the degree of the nonuniqueness for the solution in the inversion process will be alleviated by narrowing down the search region in the Bayesian retrieval technique. We will compare the precipitation detection performance and the retrieval result from the single database and that from stratified databases throughout this paper.

2. Data

The primary data used in this study include 5 min, 1 km gridded National Mosaic and Multi-Sensor Quantitative Precipitation Estimation (NMQ) [*Zhang et al.*, 2011] and Special Sensor Microwave Imager/Sounder (SSMIS) data sets [*Yan and Weng*, 2008] with 13 TBs at frequencies of 19.4 (V/H), 22.2 (V), 37.0 (V/H), 52.8 (V), 54.4 (V), 91.7 (V/H), 150.0 (H), 183.3 $\pm$ 1 (H), 183.3 $\pm$ 3 (H), and 183.3 $\pm$ 7 (H) GHz (V = vertical and H = horizontal polarizations). Hereafter, these channels will be referred to as H19, V19, …, H183 $\pm$ 7 for convenience. Data from 2010 to 2013 are used over the land portion of the domain from 25°–50°N, 70°–130°W.

It is worth mentioning that four *Z-R* relationships are utilized to link the radar reflectivity and precipitation rate in the NMQ product, i.e., $Z = 300R^{1.4}$, $Z = 200R^{1.6}$, $Z = 230R^{1.25}$, and $Z = 75R^{2.0}$ for convective, stratiform, warm rain, and snowfall, respectively. The justification for using separate *Z-R* relation for different cloud systems are provided by *Zhang et al.* [2011]. Additionally, previous work [*Chen et al.*, 2013; *Tang et al.*, 2014] showed that there exist biases in the NMQ rain rates over the targeted regions in this study, compared with rain gauge-corrected observations (e.g., Stage IV precipitation products). However, the NMQ precipitation has the highest temporal resolution (5 min), which ensures that enough matched-up samples are obtained. We would like to clarify that the purpose of this study is not to define the climatology of precipitation using the NMQ data. Instead, we use the NMQ observations as the common ground reference to compare the precipitation retrieval results from the single database to that from stratified databases.

Ancillary data sets employed in this study include surface type derived from clear-sky microwave climatology emissivity TELSEM [*Aires et al.*, 2011], Modern-Era Retrospective Analysis for Research and Applications (MERRA) reanalysis data [*Rienecker et al.*, 2011], and land elevation [*Hastings and Dunbar*, 1998]. The entire globe is divided into 11 surface types based on the monthly clear-sky emissivity from multisensor observations, and the monthly surface type index is gridded at 0.25° spatial resolution. The relative humidity, vertical velocity, geopotential height, and temperature profiles from MERRA reanalysis data are provided eight times daily at an approximate 0.5° resolution from the 3-D instantaneous state on pressure level data product and every hour for surface temperature data from the 2-D surface and radiation flux data product. The freezing level height has also been calculated from MERRA reanalysis data set. Similarly to *Harris et al.* [2000], linear interpolation of the temperature profile at each grid point is utilized to find the geopotential height of the 0°C isotherm, and then the corresponding geopotential height is taken as the freezing level height for that grid. The Global Land One-Kilometer Base Elevation was provided by the National Geophysical Data Center of National Oceanic and Atmospheric Administration (NOAA).

The spatial resolutions among various SSMIS channels are different, and they also differ from the NMQ resolution. To analyze coincident data from all these channels, data collocation was performed, as follows. First, the resolution at V37 (31 $\times$ 41 km) is taken as the nominal resolution. The nine closest pixels at higher frequencies from 91 GHz to 183.3 $\pm$ 7 GHz are chosen, and then the TBs from these nine pixels are simply averaged to represent the TBs for the aforementioned higher frequencies at the 37 GHz resolution. For lower frequency channels (i.e., 19 GHz and 22 GHz) their original coarser spatial resolution has been used in this study. That is, the closest neighbor pixel to the V37 GHz pixel is chosen. Many resolution enhancement techniques have been developed in the past [e.g., *Farrar and Smith*, 1992; *Bauer and Bennartz*, 1998; *Rapp et al.*, 2009]. While these approaches bring better matching resolution among all the channels, they also introduce noise by the

resolution enhancement. In this study, we decided to work with the original resolution for data at the lower frequencies. This collocation process is similar to that by *Viltard et al.* [2006] and *You et al.* [2011]. The precipitation rates at the closest 1271 (31×41) NMQ 1 km grid points to each 37 GHz pixel are simply averaged, which is taken as the precipitation rate at the 37 GHz resolution. For all other data (surface type, surface temperature, and land elevation), we use data from the closest grid. Temporally, surface temperature, vertical velocity, and relative humidity temperature profiles are linearly interpolated to match the time of the TB observation.

3. Methodology

As mentioned in section 1, one of the unique features in our retrieval algorithm is to make both the surface condition and precipitation vertical structure as similar as possible in detection and retrieval processes. Toward this end, in the detection, three parameters (land surface type, surface temperature, and land elevation) are used to stratify the single database into many smaller but more homogeneous categories. The linear discriminant analysis (LDA) technique is then employed to detect the precipitation. In the retrieval, one more parameter (i.e., the ice layer thickness), calculated from the difference between the storm top height and the freezing level height, is used to stratify the single database first, and then the Bayesian algorithm based on the principal component analysis is used for precipitation retrieval. More information regarding the parameters selection and effectiveness will be discussed in the following sections.

Similar to *Aonashi et al.* [2009], in the radiometer-only retrieval algorithm, the storm top height is estimated by TBs. In this work, the TB difference (V19 − V91) is utilized to estimate the storm top height through a simple regression technique. Then the ice layer thickness is computed by the storm height minus the freezing level height (FLH), where FLH is obtained from MERRA temperature and geopotential height profiles. Using TBs at higher frequencies (e.g., H150 and H183 ± 7) will generate similar ice layer thickness indices.

3.1. Linear Discriminant Analysis

The linear discriminant analysis (LDA) approach is used for both rainfall and snowfall detection in the present study. In essence, the LDA approach condenses a large number of variables into one single variable while keeping as much discriminatory information as possible. To put it into perspective, suppose there exist two training databases (e.g., rain versus nonrain databases), which contain multivariables $\boldsymbol{y}$ (e.g., TBs, relative humidity, and vertical velocity) in each database. According to *Wilks* [2011] the linear discriminant function to distinguish these two groups is

$$\delta_1 = \boldsymbol{a}' \times \boldsymbol{y} \tag{1}$$

where $'$ stands for the transpose and $\boldsymbol{a}$ is the discriminant vector, calculated in the following way:

$$\begin{aligned} \boldsymbol{a} &= [\boldsymbol{S}_{\text{pool}}^{-1}](\bar{\boldsymbol{y}}_1 - \bar{\boldsymbol{y}}_2) \\ [\boldsymbol{S}_{\text{pool}}] &= \frac{n_1 - 1}{n_1 + n_2 - 2}[\boldsymbol{S}_1] + \frac{n_2 - 1}{n_1 + n_2 - 2}[\boldsymbol{S}_2] \end{aligned} \tag{2}$$

where $\bar{\boldsymbol{y}}_i$ and $\boldsymbol{S}_i$ $(i = 1, 2)$ represent the mean vector and covariance of each group, respectively. The bold symbols stand for a vector throughout this paper, and n_1 and n_2 are the samples size in these two groups, respectively.

Similar to the name convention of the scattering index (SI), the linear discriminant function (δ) computed from equation (1) is referred to as discriminant index (DI) hereafter.

It has been shown by *Turk et al.* [2013] that the DI outperforms the widely used SI method [*Grody*, 1991] for rainfall detection, especially in winter months.

3.2. Principal Component Analysis-Based Bayesian Algorithm

The current widely used Bayesian retrieval algorithm for precipitation and clouds can be dated back at least to *Rodgers* [1976] and *Lorenc* [1986]. To be consistent with the symbols used in the precipitation retrieval community, we will use x to represent the precipitation rate and $\boldsymbol{T}$ to represent the TBs. In order to obtain x, one can apply Bayes' theorem:

$$\begin{aligned} f(x|\boldsymbol{T}) &= \frac{f(\boldsymbol{T}|x) \times f(x)}{f(\boldsymbol{T})} \\ &= \frac{f(\boldsymbol{T}|x) \times f(x)}{\int f(\boldsymbol{T}|x) \times f(x) \mathrm{d}x} \end{aligned} \tag{3}$$

where $f(x|\boldsymbol{T})$ stands for the posterior probability density function (PDF) of x given the measured $\boldsymbol{T}$, $f(x)$ is the prior PDF of x, and $f(\boldsymbol{T}|x)$ is the likelihood function of $\boldsymbol{T}$ given the precipitation rate x. Equation (3) serves the foundation of Bayesian retrieval algorithm [e.g., *Evans et al.*, 1995; *Kummerow et al.*, 1996; *Chiu and Petty*, 2006; *Noh et al.*, 2006; *Kim et al.*, 2008; *Munchak and Skofronick-Jackson*, 2013; *Sano et al.*, 2013; *Petty and Li*, 2013].

From equation (3), there exist two ways to obtain the expected value of x, given $\boldsymbol{T}$. One way [e.g., *Evans et al.*, 1995; *Chiu and Petty*, 2006] draws samples from the posterior PDF. The other way directly uses the likelihood function and the prior PDF to calculate the expected value of x, given $\boldsymbol{T}$, without knowing the form of the posterior PDF [e.g., *Kummerow et al.*, 1996; *Evans et al.*, 2002; *L'ecuyer and Stephens*, 2002]. The details of the latter approach can be mathematically stated as follows:

$$\begin{aligned} E[x|\boldsymbol{T}] &= \int x f(x|\boldsymbol{T})\mathrm{d}x \\ &= \frac{\int x \times f(\boldsymbol{T}|x) \times f(x)\mathrm{d}x}{\int f(\boldsymbol{T}|x) \times f(x)\mathrm{d}x} \\ &= \frac{E[x \times f(\boldsymbol{T}|x)]}{E[f(\boldsymbol{T}|x)]} \end{aligned} \tag{4}$$

where E stands for the expectation. Using samples from prior PDF can be particularly convenient when there exists a predefined database, from either observations or model simulations. In this study, we use this procedure to calculate the expected value of the precipitation rate, given $\boldsymbol{T}$.

In addition, the likelihood function is usually assumed to follow a multivariate normal distribution, and the TBs are assumed uncorrelated; therefore, the covariance matrix is diagonal [e.g., *Rodgers*, 1976; *Evans et al.*, 1995; *Kummerow et al.*, 1996; *Austin et al.*, 2009; *Evans et al.*, 2012]. However, it is known that the TBs at different channels often are highly correlated. In lieu of this, we first apply the principal component analysis (PCA) to the TBs for a given precipitation rate. Instead of using the TBs directly, we will use the first three leading PCs in the Bayesian framework, which account for approximately 98% of total variance. In this study, we will use $\boldsymbol{u}$ to represent the principal components. Details regarding the PCA technique is referred to *Wilks* [2011].

In our method, the log transformation has been applied to precipitation x and they are placed into n small bins. Depending on the sample size in the database, n should be adjusted to ensure retrieval accuracy. In each bin, we use $L_1, \ldots, L_n$ to represent the sample size, and $x_1, \ldots, x_n$ to represent the mean value of the precipitation rate.

In each small bin (i.e., corresponding to each x_i), the PCA technique is applied to the TBs. Next, we use equation (4) by replacing the TB variables ($\boldsymbol{T}$) by principal components ($\boldsymbol{u}$):

$$\begin{aligned} E(x|\boldsymbol{u}) &= \frac{\int x \times f(\boldsymbol{u}|x) \times f(x)\mathrm{d}x}{\int f(\boldsymbol{u}|x) \times f(x)\mathrm{d}x} \\ &= \frac{E[x \times f(\boldsymbol{u}|x)]}{E[f(\boldsymbol{u}|x)]} \\ &= \frac{\sum_{i=1}^{n} L_i \times x_i \times \chi_{ik}^2}{\sum_{i=1}^{n} L_i \times \chi_{ik}^2} \\ \chi_{ik}^2 &= \prod_{k=1}^{K} \frac{1}{\sqrt{2\pi}\sigma_{ik}} \exp\left(-\frac{1}{2}\frac{(u_k - \mu_{ik})^2}{\sigma_{ik}^2}\right) \end{aligned} \tag{5}$$

where n represents the number of the precipitation bins; K is the number of the principal components; L_i and x_i are the sample size and the mean precipitation rate in the ith precipitation bin, respectively; u_k is the kth principal component; and μ_{ik} and σ_{ik} stand for the mean and standard deviation of the kth principal component in the ith precipitation bin, respectively.

In this study, the number of the bins is 100 (i.e., $n = 100$) and the number of the leading PCs is 3 (i.e., K=3). More details regarding the PCA-based Bayesian retrieval algorithm is referred to *You* [2013].

Table 1. Notation for Precipitation/No-Precipitation Results Judged by NMQ and SSMIS

	Precipitation Judged by NMQ	No Precipitation Judged by NMQ
Precipitation judged by SSMIS	*a*	*b*
No precipitation judged by SSMIS	*c*	*d*

4. Precipitation Detection

In this section, the performance of the LDA for precipitation detection is investigated. We first determine the precipitation type (rainfall or snowfall) by checking whether the 2 m air temperature is greater than 0°C. It is concluded by *Liu* [2008] that this threshold is rather conservative, which corresponds to a 90% rain to snow transition probability based on multiyear ground observations. The threshold for the minimum detectable precipitation rate is assigned to be 0.22 mm/h, according to *Munchak and Skofronick-Jackson* [2013]. Then the rain/no-rain and snow/no-snow databases are constructed separately.

For precipitation detection, three parameters (surface type, surface temperature, and land elevation) are employed to stratify the single database into many smaller but more homogeneous databases. It is worth mentioning that these three parameters are not chosen randomly. The surface temperature and surface type (derived from emissivity climatology) largely reflects the background emission from the land surface. Additionally, *Gebregiorgis and Hossain* [2013] showed that the uncertainties in the satellite-derived rainfall product has clear dependence on the elevation, and therefore, it is worthwhile to assimilate this information into the precipitation retrieval algorithm.

The performance of the precipitation detection is measured by the probability of detection (POD) and false alarm rate (FAR), which are defined by the following equations according to *Wilks* [2011]:

$$\begin{aligned} \mathrm{POD} &= \frac{a}{a+c} \\ \mathrm{FAR} &= \frac{b}{b+d} \end{aligned} \tag{6}$$

where the definitions for *a*, *b*, *c*, and *d* are referred to Table 1.

By changing the threshold value for the DI, the corresponding POD to the FAR at 0.05 for rainfall and 0.10 for snowfall is used to judge the performance of the precipitation detection. Larger POD indicates better precipitation detection performance. A detailed example will be provided in the next section to show how exactly this approach works. It is worth mentioning that the FAR threshold numbers (0.05 for rainfall and 0.10 for snowfall) are selected somewhat arbitrarily. Choosing other thresholds will only affect the numerical values of the statistics in the following study, not the conclusions. In reality, the thresholds should be adjusted depending on different applications (e.g., drought versus flood monitoring).

4.1. Single Database Versus Stratified Databases for Precipitation Detection

Basically, there are two possible ways to judge an observed pixel as a precipitation or no-precipitation pixel. One way is to compare this pixel with all the historical pixels in the single historical database. Alternatively, based on the surface type, surface temperature, and land elevation, one could first find which stratified database this pixel belongs to. Then this pixel is only compared with that in the same stratified database. For example, it is well known that the microwave radiometric signature from different surface backgrounds (e.g., forest, desert, and snow/ice-covered land) differs greatly. Therefore, it is better to compare a newly obtained observation over desert with only the historical observations over desert. In this section, we will use real observations to demonstrate that the latter philosophy is more effective for precipitation detection.

For rainfall detection, the original surface types are regrouped into 5 categories due to data sample size issue, including dense vegetation (1), medium vegetation (2), sparse vegetation (3–5), ice and snow–covered land (6–9), and coast (10). The numbers in parentheses are the original surface type index in the emissivity climatology database [*Prigent et al.*, 2006]. The surface temperature is grouped into three categories. The thresholds are the values corresponding to 33.3% and 66.7% of the surface temperature. The land elevation is divided into two categories using 500 m as the threshold. Using these three parameters, the single database for rainfall detection can then be stratified into 30 smaller groups.

To make the reader familiar with the LDA precipitation detection technique, we show the histograms of the DI derived from the single rain/no-rain database in Figure 1. For visual inspection, each histogram is scaled

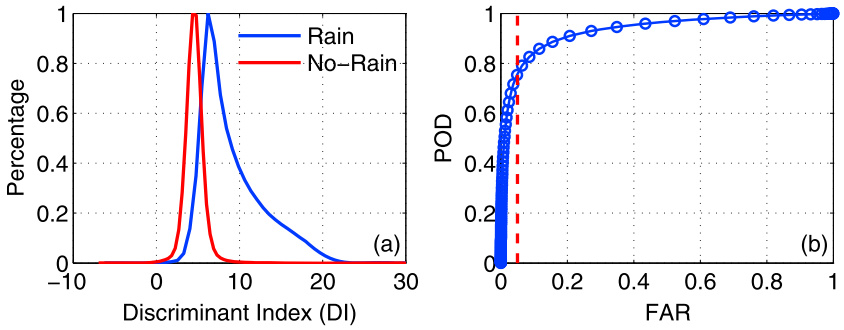

Figure 1. (a) Histograms of the discriminant index (DI) derived from the single database for nonraining (red line) and raining scenes (blue line). Both histograms have been scaled by the corresponding maximum value in each histogram. (b) Probability of detection (POD) versus false alarm rate (FAR) by choosing different thresholds for DI. The red dashed line stands for the FAR at 0.05.

by its maximum value of the corresponding histogram. Figure 1a shows the histograms of the DI for rain and nonrain scenarios in the single database, which are overlapped. By choosing different critical values of DI for rain detection from −10 to 30, many corresponding PODs and FARs are obtained from equation (6), shown in Figure 1b, where the red dashed line represents FAR at 0.05. It can be seen that the POD is directly proportional to FAR. In this study, the corresponding POD to the FAR at 0.05 (0.10) is selected for rainfall (snowfall) to judge the detection performance. Again, we would like to emphasize that both threshold values (0.05 for rainfall and 0.10 for snowfall) are selected somewhat arbitrarily and should be adjusted for different applications. However, choosing different values will not change the conclusions in this study.

For rainfall detection using the single database, the POD is 75.9% using the training data set from 2010 to 2013. The average POD from 30 stratified rainfall databases is increased by 8.1% to 84.0% when applying the LDA to stratified databases (Table 2). The similar detection procedure is applied to the snowfall. It is found that by stratifying the single database, the POD increases 12% from 56.0% to 68.0% for snowfall detection (Table 3). It is worth mentioning that we group the single database into 12 smaller categories for snowfall detection due to data availability issue, by dividing the original surface type into vegetation (1–5), ice and snow–covered land (6–9), and coast (10); the temperature into two categories (less or greater than 268 K, the 50.0% value); and the elevation into two categories (less or greater than 500 m).

To summarize, by using the stratified databases, the POD increases approximately 8.1% and 12.0% for rainfall and snowfall detection, respectively.

4.2. Influence of Other Environmental Parameters to the Precipitation Detection

Besides the surface type, surface temperature, and land elevation, which have been used to stratify the single database into many more homogeneous databases for precipitation detection, previous work also showed that several other large-scale environmental parameters may also be related to the precipitation process to a certain degree. These parameters include average relative humidities at lower troposphere from 1000 hPa to 700 hPa and at higher troposphere from 700 hPa to 300 hPa, vertical velocities at 500 hPa and 700 hPa, surface equivalent potential temperature, moisture flux 50 hPa above surface and convective available potential energy [*Liu and Fu*, 2001; *Hirose and Nakamura*, 2004; *Liu and Zipser*, 2013; *Smith et al.*, 2013]. These parameters could also be used to further stratify the single database. However, by doing this, the number of the categories will increase dramatically and the sample size will be too small in each category to perform meaningful statistical analysis. Instead of further stratifying the databases, the aforementioned seven parameters

Table 2. Probability of Detection (POD, %) for Rainfall From the Single Database or Stratified Database, and With/Without Considering the Vertical Velocity (ω) at 700 hPa and the Relative Humidity (rh) at the Lower Troposphere (1000–700 hPa)

	Without (ω, rh)	With (ω, rh)
Single database	75.9	78.5
Stratified database	84.0	85.1

Table 3. As in Table 2 Except for Snowfall

	Without (ω, rh)	With (ω, rh)
Single database	56.0	67.2
Stratified database	68.0	76.4

are treated just like TBs in the LDA detection process. We are going to test how much improvement can be achieved by adding these variables (besides the TBs) in the LDA detection process.

These seven variables are added into the LDA approach in a stepwise fashion. That is, we will include the TBs, along with the first parameter, the first two parameters, until all seven parameters are included. It was found that by only adding relative humidity (rh) at lower troposphere and vertical velocity at 700 hPa (ω), the POD improvements are very similar to that by adding all seven parameters. Specifically, for rainfall detection, the POD increases from 84.0% to 85.4% by adding all seven parameters for stratified databases. On the other hand, by only adding the rh and ω, the POD is increased to 85.1%. For the single database, the PODs are almost identical with only 0.2% difference between adding all seven variables and adding only rh and ω variables. For snowfall detection, the POD positive difference between adding seven variables and adding two variables (rh and ω) is 1.5% and 1.7% for using the single database and stratified database, respectively. Therefore, we decided that only these two variables (relative humidity at the lower troposphere and vertical velocity at 700 hPa) are kept for further analysis. The relative humidity at the lower troposphere represents the degree of the saturation of the large-scale environmental background. Higher relative humidity is generally associated with larger possibility of precipitation. In addition, the vertical velocity at 700 hPa represents the instability of the large-scale environment. In general, strong upward motion (i.e., large negative vertical velocity) is indicative of possible precipitation.

It is shown in Table 2 that the relative humidity and vertical velocity have relatively weaker influence for rainfall detection. The PODs only increase from 75.9% to 78.5% for the single database and from 84.0% to 87.6% for stratified databases. In contrast, for snowfall detection the PODs increase by 11.2% from 56.0% to 67.2% for the single database and 8.4% from 68.0% to 78.4% for stratified databases by adding these two variables (Table 3). It is hypothesized that the large-scale factors (relative humidity and vertical velocity) play more important roles in the snowfall genesis, which tends to be more stratiform in nature, compared with that in the rainfall genesis, which may include both stratiform and convective types.

To summarize, it is demonstrated that by using the stratified databases and adding the relative humidity at lower troposphere and vertical velocity at 700 hPa, the POD increases by 20.4% from 56.0% to 76.4% for snowfall detection. For rainfall detection, using stratified databases, the POD increases 8.1% from 75.9% to 84.0%. However, by adding the two large-scale environmental variables (rh and ω), the POD improvement is relatively small. Particularly, it increases by 2.6% from 75.9% to 78.5% using the single database and by 1.1% from 84.0% to 85.1% using stratified databases. Therefore, for rainfall detection, only the TBs are considered in the LDA techniques, while the relative humidity at lower troposphere and vertical velocity at 700 hPa are included besides the TBs for snowfall detection.

The detection statistics are summarized in Tables 2 and 3. It is worth mentioning that all these analyses are based on the training data set from 2010 to 2012. Similar analyses are conducted using the validation data set (2013), and very similar detection performances are obtained.

In addition, we would like to emphasize that only the clear-sky radiances (i.e., TBs) are assimilated into the MERRA reanalysis data set. And the relative humidity and vertical velocity are purely from the model output, which have not been adjusted by the simultaneous satellite observations. Therefore, the improvement, by including these two variables in the precipitation detection process, is unlikely caused by the redundant use of the TBs within the MERRA data and the LDA method.

5. Precipitation Retrieval

5.1. Effectiveness of Categorizing Parameters

To construct the rainfall and snowfall databases for precipitation rate retrieval, four parameters (surface type, surface temperature, land elevation, and ice layer thickness) are used to stratify the single database.

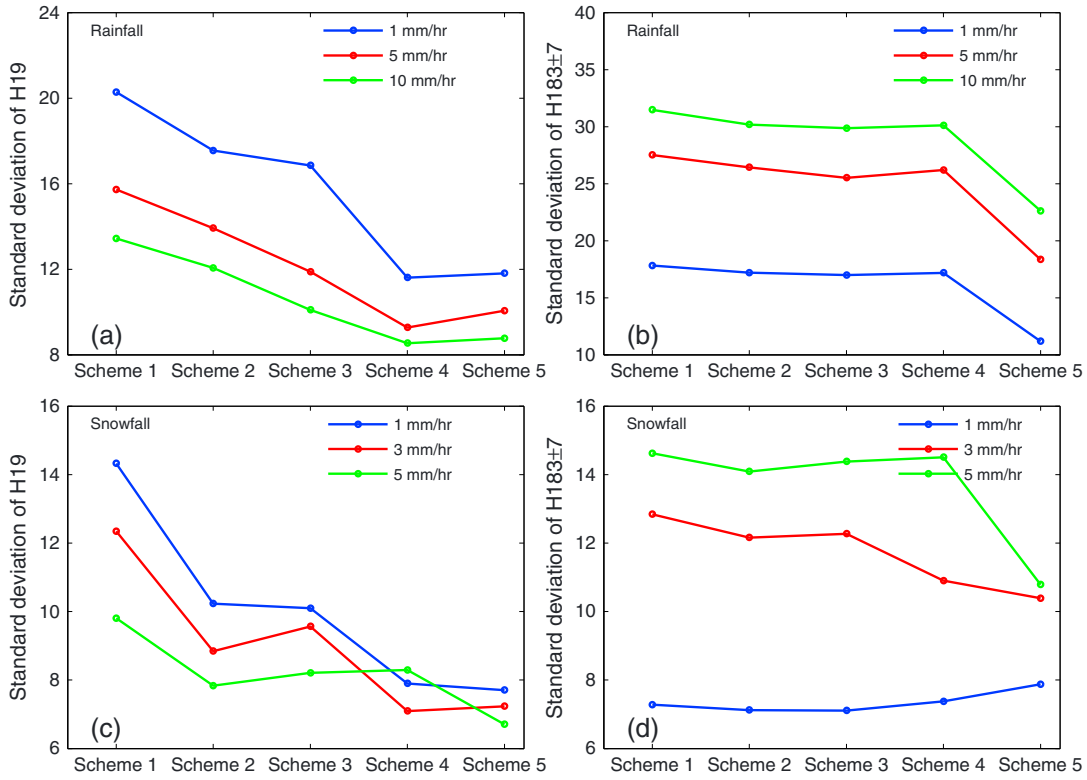

Figure 2. (a) Under different scheme designs, standard deviation of brightness temperature at H19 corresponding to 1, 5, and 10 mm/h surface rain rate. Schemes 1–5, in order, stand for using the single database, using databases stratified by one parameter (surface type), using databases stratified by two parameters (surface type and surface temperature), using databases stratified by three parameters (surface type, surface temperature, and land elevation), and using databases stratified by four parameters (surface type, surface temperature, land elevation, and ice layer thickness). (b) Same as Figure 2a except at H183 ± 7. (c) Same as Figure 2a except for snowfall corrsponding to 1, 3, and 5 mm/h surface snow rate. (d) Same as Figure 2c except at H183 ± 7.

The primary objective is to make sure that both the surface condition and precipitation vertical structure are as similar as possible in each stratified database. In other words, for the same surface rain rate, the variation of the TBs in the stratified databases should be smaller compared with that in the single database. TBs at H19 and H183 ± 7 are selected to illustrate the effectiveness of the aforementioned four parameters, since these two channels are the most sensitive indicators to the surface condition and precipitation vertical structure, respectively.

We compared the standard deviation in the single database and the mean of the standard deviations in stratified databases, corresponding to the same surface rain rate. The comparison is performed in a stepwise fashion. First, the standard deviations of the TBs at H19 and H183 ± 7 are computed in the single database, corresponding to 1, 5, and 10 mm/h surface rain rate. Next, the surface type is used to stratify the single database. There are five and three smaller databases for rainfall and snowfall when the surface type is used to stratify the single database, respectively. In each smaller database, the standard deviation of the TB at H19 is calculated and then the mean of these standard deviations are obtained. Further stratification is conducted by adding other three parameters one by one. For convenience, only using the single database for standard deviation calculation is named as scheme 1; databases stratified by surface type as scheme 2; databases stratified by surface type and surface temperature as scheme 3; databases stratified by surface type, surface temperature, and land elevation as scheme 4; and databases stratified by surface type, surface temperature, land elevation and ice layer thickness as scheme 5.

The result is shown in Figure 2. It is obvious that corresponding to 1 mm/h rainfall (Figure 2a), the standard deviation of H19 decreases from 20 to 12 by using the surface type, surface temperature, and land elevation (i.e., from scheme 1 to scheme 4), while the ice layer thickness parameter appears to have very little influence on the standard deviation of H19 (scheme 5), as we have expected. Similar variation reduction characteristics at H19 are observed corresponding to 5 and 10 mm/h surface rain rate (Figure 2a). On the other hand, corresponding to the same surface rain rate (i.e., 1, 5, and 10 mm/h), a large decrease of the standard deviation at

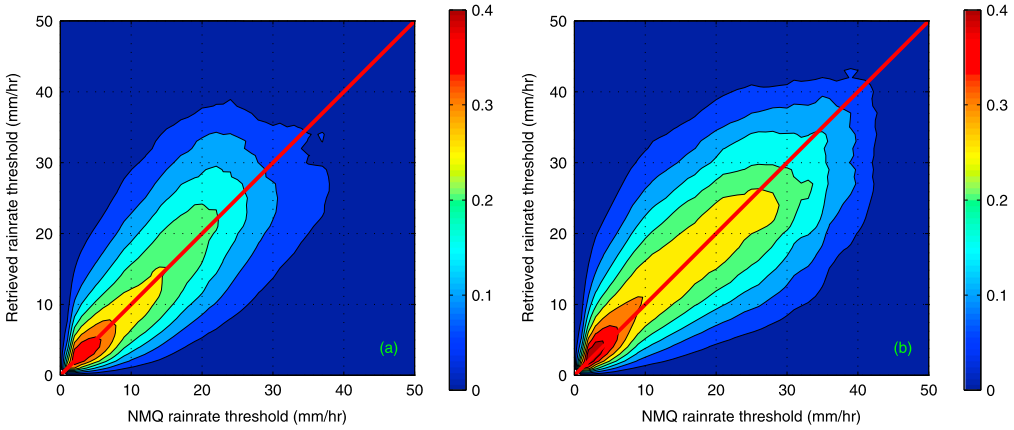

Figure 3. Two-dimensional Heidke Skill Score (HSS) plot to quantify the correspondence between NMQ and SSMIS instantaneous rain rate estimates in 2013. (a) The rain rates are estimated from the single database. (b) The rain rates are estimated from stratified database.

H183 ± 7 is observed only after including the ice layer thickness parameter, while the other three parameters have very little influence on the TB at H183 ± 7 (Figure 2b).

For snowfall, a similar result is found when applying these four parameters to snowfall databases (Figures 2c–2d). For example, corresponding to 1 mm/h snow rate, the standard deviation of the TB at H19 in the single database is approximately 14 (scheme 1), while the standard deviation in the stratified databases (scheme 4) is reduced to 8. However, for snowfall we would like to point out that the standard deviation at H183 ± 7 GHz shows little variation corresponding to 1 mm/h snowfall, even after using the ice layer thickness parameter. It is hypothesized that the water vapor probably masks out the signal from ice scattering when the snowfall rate is 1 mm/h. The decrease of the standard deviation at H150 is evident, even for 1 mm/h snowfall (not shown).

In summary, it is concluded that compared with the single database, the four selected parameters (surface type, surface temperature, land elevation and ice layer thickness) are effective in reducing the variation of the TBs, corresponding to the same surface rain rate. Specifically, the first three parameters (surface type, surface temperature, and elevation) largely characterize the surface condition, while the ice layer thickness parameter largely captures the precipitation vertical structure information.

5.2. Results From Single Database Versus Those From Stratified Databases

To compare the performance of precipitation retrieval by using the single database or stratified databases, the widely used 2-D Heidke Skill Score (HSS) [*Conner and Petty*, 1998; *McCollum and Ferraro*, 2003; *Liu and Seo*, 2013] is shown in Figure 3 for rainfall retrieval result. The 2-D HSS plot shows the probability distribution of the retrieved rain rates, taking the NMQ observed rain rates as references. The HSS is 1 when the retrieved

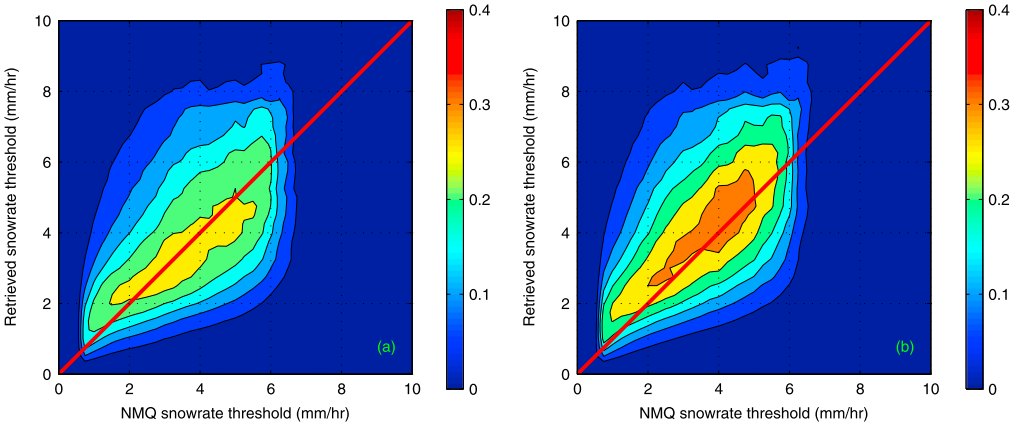

Figure 4. As in Figure 3 except for snowfall.

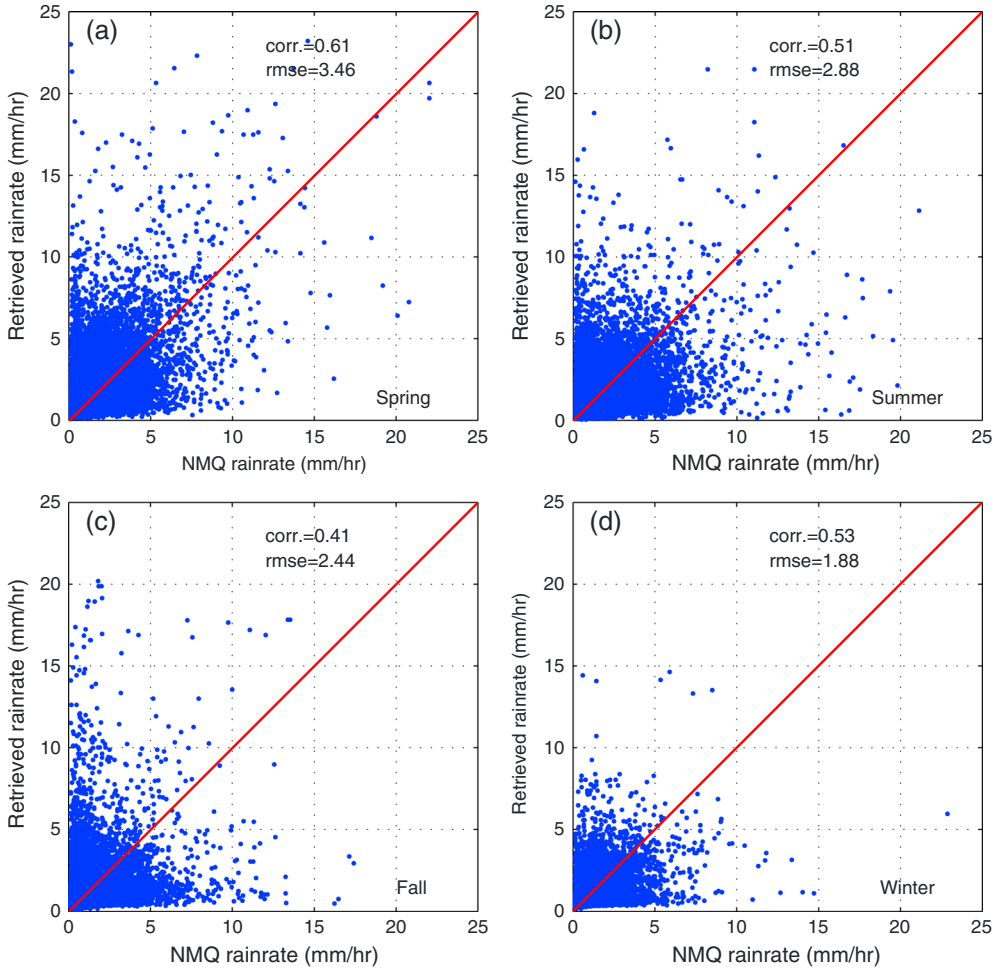

Figure 5. Scatterplot of the SSMIS estimated rain rates from stratified databases and NMQ observed rain rates at 0.1° in (a) spring, (b) summer, (c) fall, and (d) winter.

precipitation rates perfectly match the observations. On the other hand, the HSS is 0 when the retrieved precipitation rate behaves randomly corresponding to observed precipitation rates. The superiority (larger HSS) of the retrieved rain rate using the stratified databases is readily observed, especially when rain rate is less than 3 mm/h or greater than 20 mm/h. Physically speaking, the larger HSS indicates that the retrieved rain rates using the stratified databases more likely agree with the observations. In particular, using the single database, there is no skill at all when the rain rate is larger than 35 mm/h (Figure 3a), whereas the stratified database exhibits limited skill at the extreme condition. In Figure 4, a similar plot is shown for snowfall retrieval result. The retrieved result from stratified databases outperforms that from the single database, indicated by the larger HSS from 0 to 8 mm/h.

We have also analyzed the retrieved results by comparing the observed and retrieved precipitations at 0.1° resolution, shown in Figures 5 and 6. The correlation between retrieved and observed rain rates increases from 0.42 for the single database to 0.63 for stratified databases. On the other hand, the root-mean-square error (rmse) decreases approximately 53.2% from 2.07 to 0.98 when stratified databases are used. Figure 5 shows the scatterplots between NMQ observed rain rates and retrieved rain rates from SSMIS from all four seasons, using stratified databases. Compared with the results from the single database (Figure 6), it is clear that from spring to fall the retrieved rain rates from stratified databases possess larger correlations and smaller rmse. Particularly, in these three seasons the overestimation of the rain rate from the single database when the observed rain rate is less than 4 mm/h is alleviated in the result from stratified databases. This characteristic contributes greatly to the large rmse decrease from spring to fall. In the winter season, it seems the results from the single database and stratified database are comparable. However, the underestimation from the

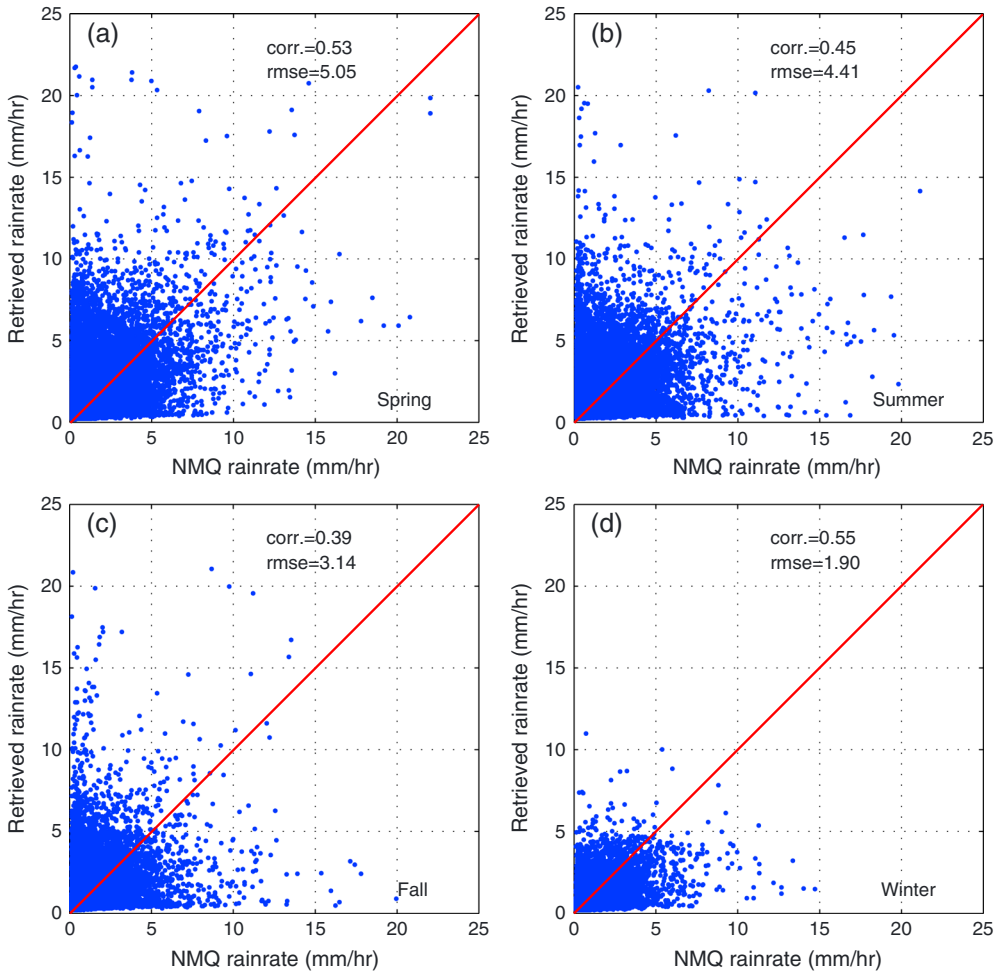

Figure 6. As in Figure 5 except estimated rain rates from the single database.

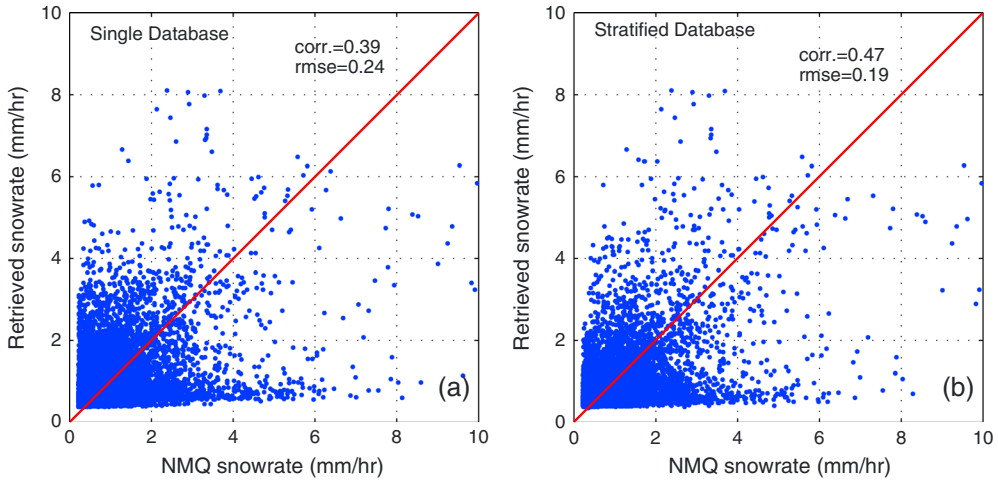

Figure 7. Scatter plot of SSMIS estimated snow rates and NMQ observated snow rates at 0.1° resolution in 2013 (a) using the single database and (b) using stratified databases.

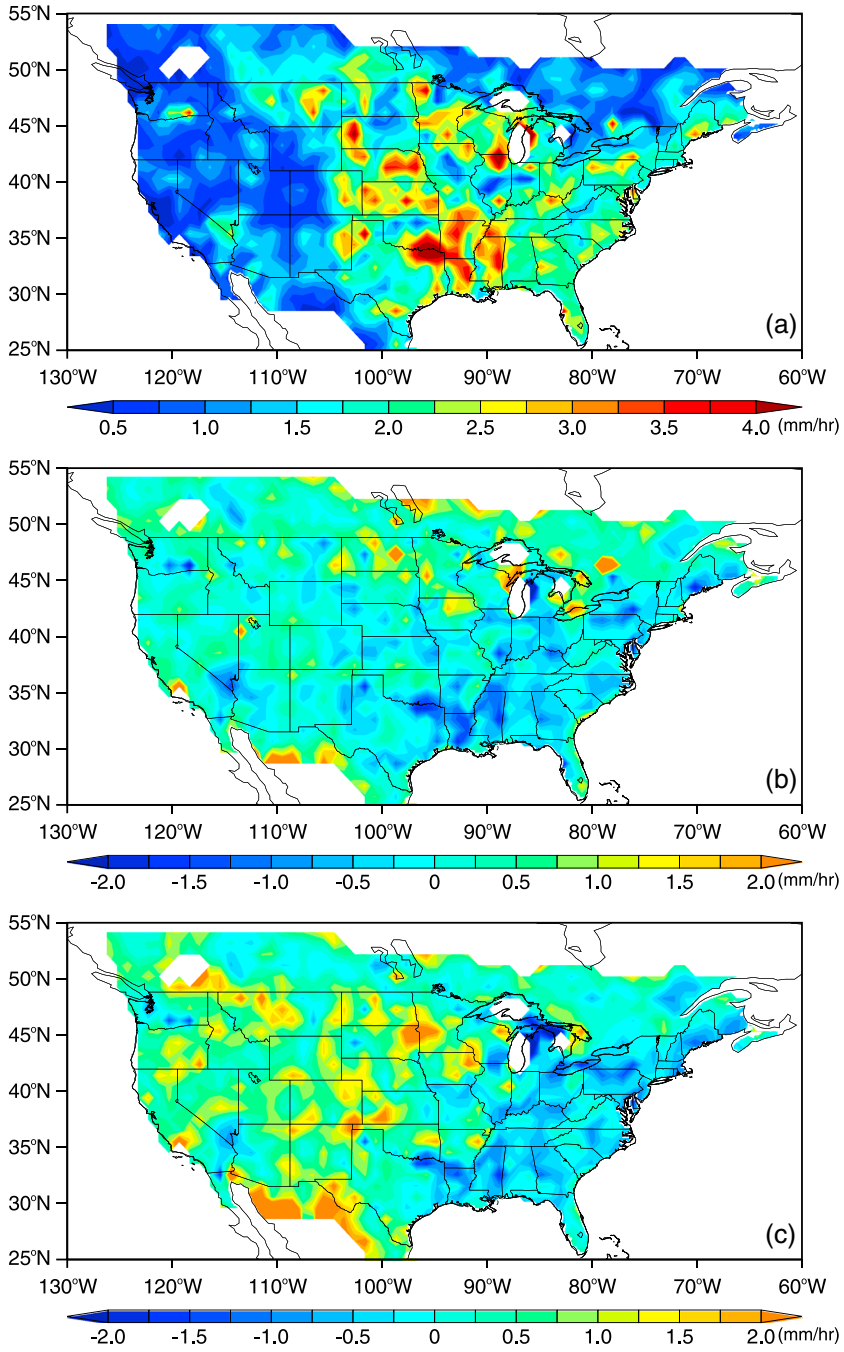

Figure 8. Geospatial distribution of the estimated and NMQ observed rain rate in the summer season (June, July, and August). (a) Average rain rates at 1° resolution from NMQ observations. (b) Differences between SSMIS estimated rain rates using stratified databases and NMQ observed rain rates. (c) Differences between SSMIS estimated rain rates using the single databases and NMQ observed rain rates.

single database is more severe when the observed rain rate is greater than 8 mm/h. In the winter season, the convective cloud systems are less frequent and not as intense as those in the other three seasons [*Zipser et al.*, 2006] over the continental United States, so the dynamic range of the rain rate is relatively smaller. When the Bayesian retrieval framework is applied, it is less likely to obtain retrieved rain rates far from observed rain rate since the Bayesian algorithm in essence is an optimal weighted average. This explains why the retrieval improvement using the stratified databases in the winter season is marginal.

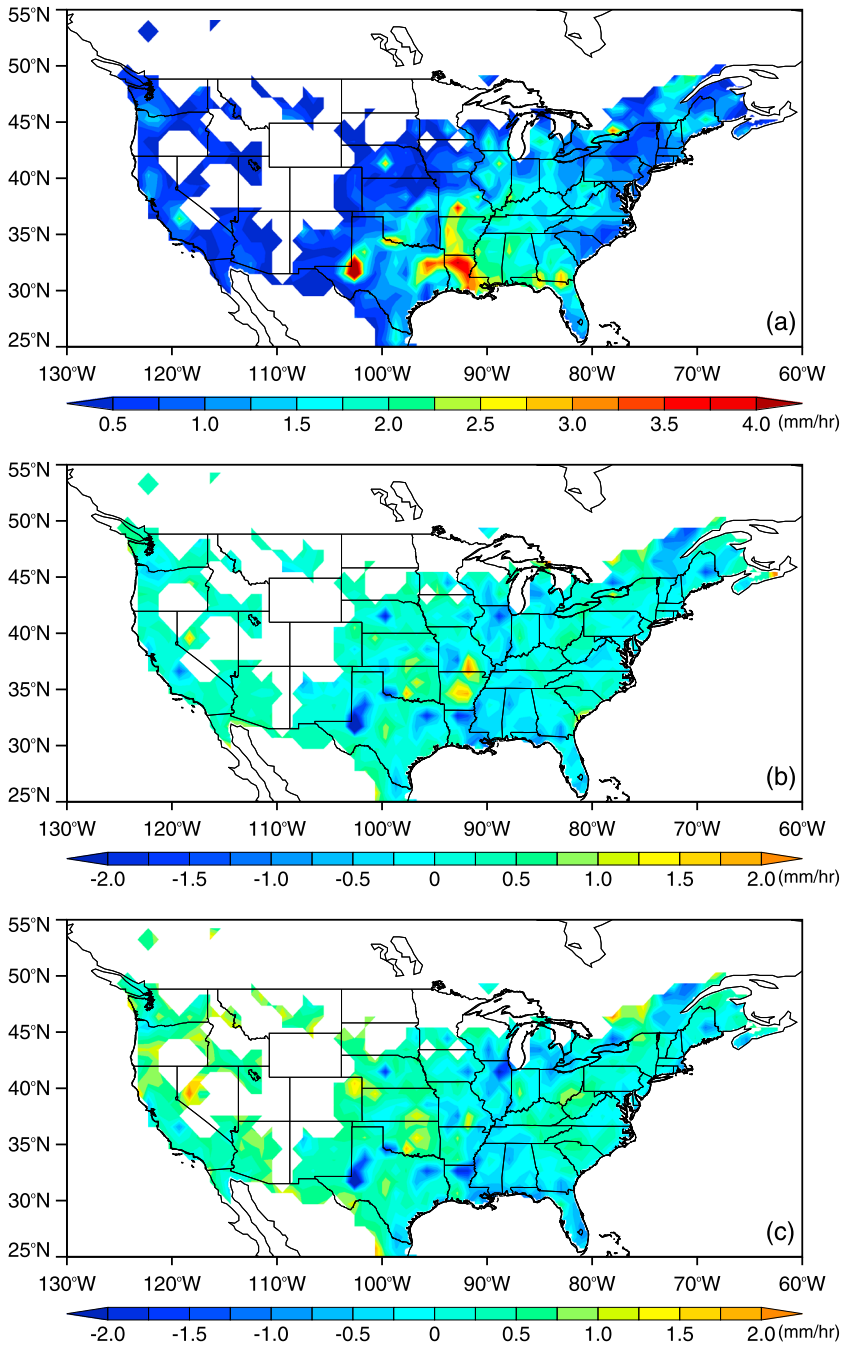

Figure 9. As in Figure 8 except in the winter season (December, January, and February).

Similar analysis has also been performed for snowfall. It is noted that using stratified databases will improve the retrieval result as indicated by increased correlation from 0.39 for the single database to 0.47, shown in Figure 7. The rmse is also reduced from 0.24 to 0.19. It is noted that the rmse deduction is relatively small, compared with that in the rainfall retrieval results from spring to fall. Again, the much smaller dynamical range of the snow rates in the database makes it less likely to produce retrieved snow rates dramatically further apart from observations.

Overall, the superior performance, indicated by larger Heidke Skill Score (HSS), is observed for the retrieved precipitation from stratified databases, compared with that from the single database. In addition, when using the stratified databases, the correlation coefficients between retrieved rain rates and observations increases

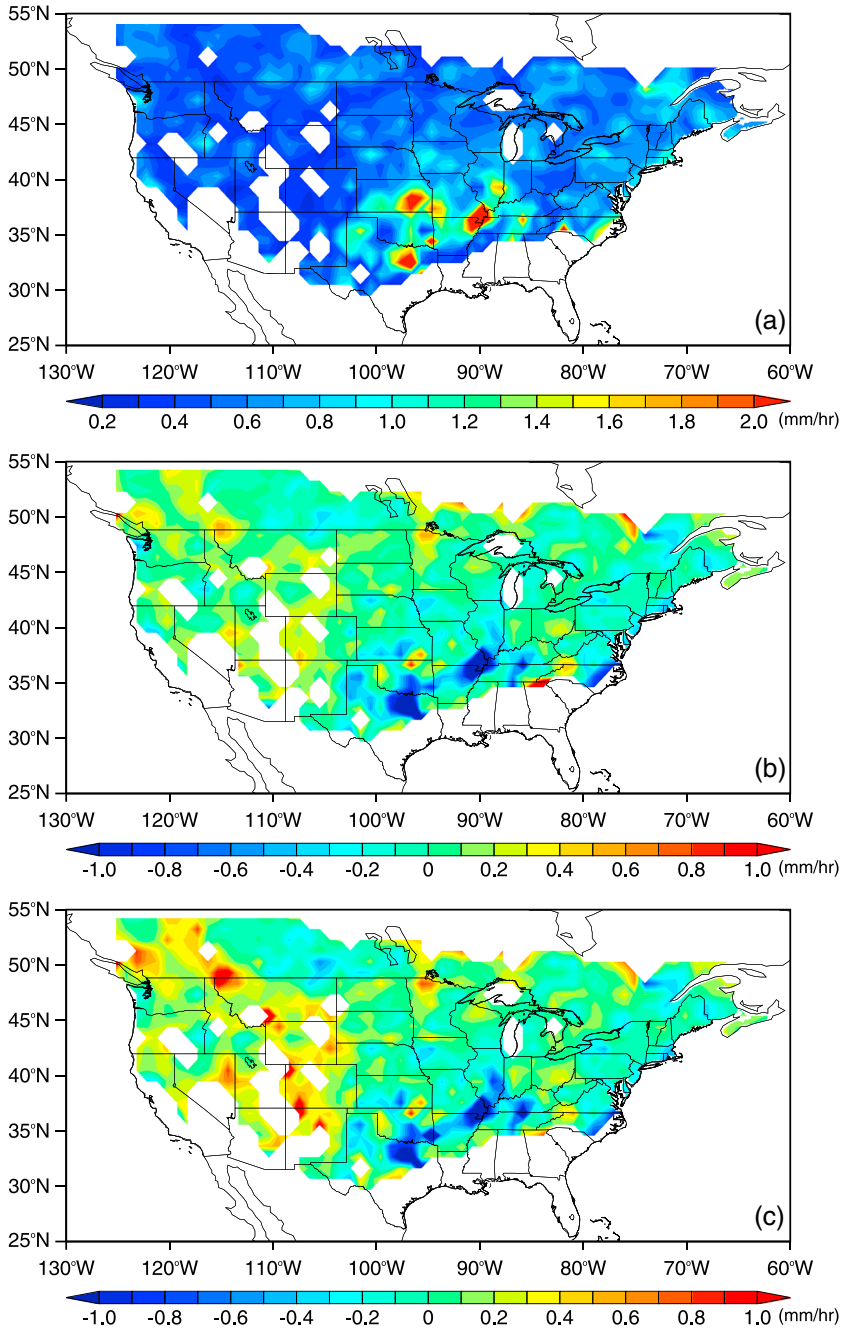

Figure 10. (a) Average snow rates at 1° resolution from NMQ observations. (b) Differences between SSMIS estimated snows using stratified databases and NMQ observed snow rates. (c) Differences between SSMIS estimated snow rates using the single databases and NMQ observed snow rates.

from 0.42 to 0.63, while the root-mean-square error decreases about 53% from 2.07 to 0.98. Noticeable improvements have also been achieved by using stratified databases for snowfall retrieval.

5.3. Spatial Distribution of the Precipitation from the Single Database and Stratified Databases

In this section, the spatial distribution of the retrieved precipitation from both the single database and stratified databases is investigated, shown in Figures 8–10, along with the NMQ observations.

Compared with the NMQ observed rain rates in summer (Figure 8a), there exists slight underestimation over the majority of the eastern United States for the retrieved rain rates from stratified databases (Figure 8b). There are also some regional overestimations over the northeast part of the study region. The underestimation

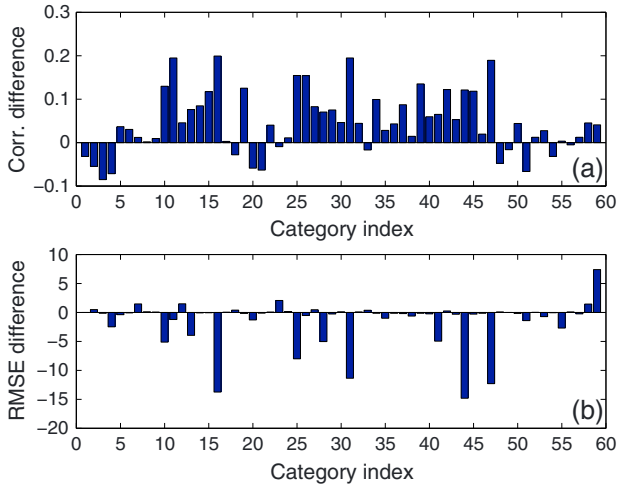

Figure 11. (a) The correlation difference between observed and retrieved rain rates from stratified databases and from the single database in each category. (b) The root-mean-square error (rmse) difference between observed and retrieved rain rates from stratified databases and the single database.

of the retrieved rain rates from the single database is also obvious over the majority of the eastern United States. Previous work [e.g., *Lin and Hou*, 2008] showed that the passive microwave sensors has the tendency to underestimate the rain rates from severe convective storms. Our results share this common problem, which is also clear in Figures 5b and 6b (rain rate > 15 mm/h). Further, the most striking feature for the retrieved rain rates from the single database is that there exist systematical overestimation from central to western United States (Figure 8c). It has long been realized that corresponding to same surface rain rate the precipitation clouds system over arid (e.g., western United States) surface background are more intense [*You and Liu*, 2012], which will lead to lower TBs. The mitigation of this overestimation in the retrieved rain rates from stratified databases is clearly indicated (Figure 8b). For the rain rate in the winter season (Figure 9), the results from the single database and stratified databases are comparable, which agrees with the results in the previous section (Figures 5d and 6d). For snowfall retrieval result, the overestimation over the western United States is clearly reduced when the stratified databases are utilized (Figure 10b).

In summary, the spatial distribution pattern of the retrieved precipitation agrees better with observed precipitation pattern when the stratified databases are used. The overestimation over the western United States is largely mitigated when the stratified databases are utilized.

Further, the geospatial pattern of the observed precipitation (Figures 8a, 9a, and 10a) is obtained by only using the matched-up samples. These patterns differ from that using all NMQ observation. More importantly, the average precipitation in1° grid box is computed based on the event occurrence, which explains why the large snowfall amount is evident in the southern United States (Figure 10a).

5.4. Necessity for Using Stratified Databases

It has been demonstrated in the previous sections that retrieved precipitation from a stratified database agrees better with observations in terms of correlation coefficient and root-mean-square error (rmse), compared with that from the single database. In this section, further analysis is conducted to investigate the underlying reasons that the stratified databases generate superior results.

The difference of the correlation coefficients between observed and retrieved rain rates from stratified databases and from the single database is shown in Figure 11a. It is noted that over majority (78%) of the categories the difference is positive, which indicates that the retrieved rain rates using stratified databases are better correlated with observations. In addition, the rmse (Figure 11b) are reduced in the vast majority of the categories.

Indeed, in some categories, using the single database will produce better rainfall retrieval results in terms of correlation and rmse. Therefore, two representative categories (categories 3 and 31) are chosen, which stand for the largest negative and largest positive correlation differences, respectively. Although the Bayesian framework is used to perform the precipitation retrieval in this study, the simple linear regression approach is used here to demonstrate the fundamental difference of using the single database or stratified databases. The TB at 183 $\pm$ 7 is selected to perform the regression analysis since it is the most sensitive indicator to the precipitation over land. Choosing other high-frequency channels (e.g., 150 and 91 GHz) will generate similar results.

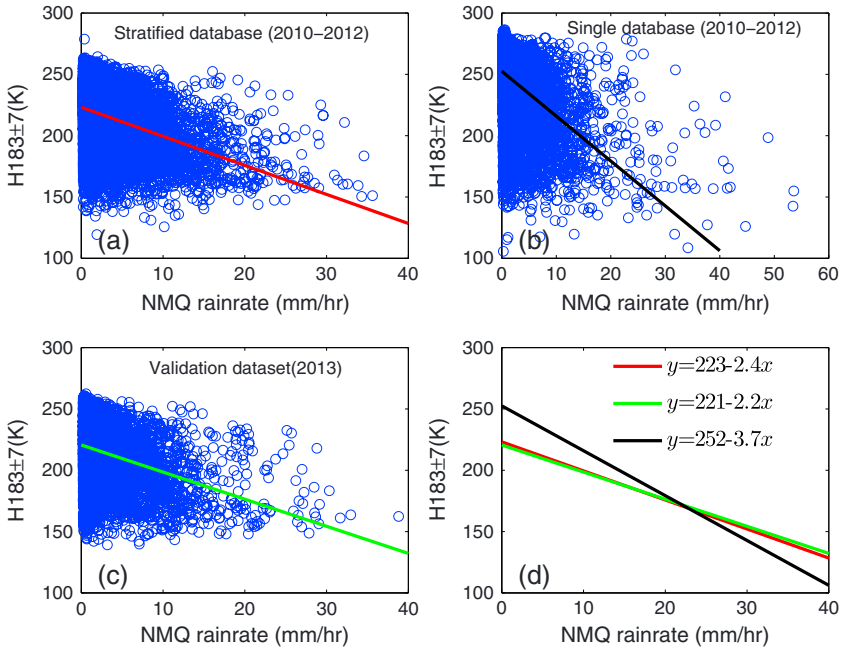

Figure 12. Regression analysis for the category in which the better result is from the stratified database. The solid line represents the fitted regression curve. (a) Scatterplot between rain rate and H183 ± 7 using the stratified database in the training data set (2010–2012). (b) Scatterplot between rain rate and H183 ± 7 using the single database in the training data set (2010–2012). (c) Scatterplot between rain rate and H183 ± 7 using the stratified database in the validation data set (2013). (d) Regression curves from training data sets in the single database and in the stratified database and from validation data set for the corresponding category.

Figures 12a and 12b show that scatterplots between rain rates and H183 ± 7 in the stratified database and single database, respectively. The solid lines stand for the linear regression curves obtained through the least squares approach. Figure 12c shows the relationship between rain rates and H183 ± 7 in the validation data set. Similarly, the solid line is the linear regression curve. These three curves are plotted together in Figure 12d, along with the regression equations. Obviously, both the slopes and the intercepts of the regression lines in the stratified databases from the training data set and the validation data sets are very close to each other (Figure 12d). In contrast, the regression curve from the single training database differs dramatically from that in the validation data set. Therefore, under this circumstance, the stratified database is preferred over the single database.

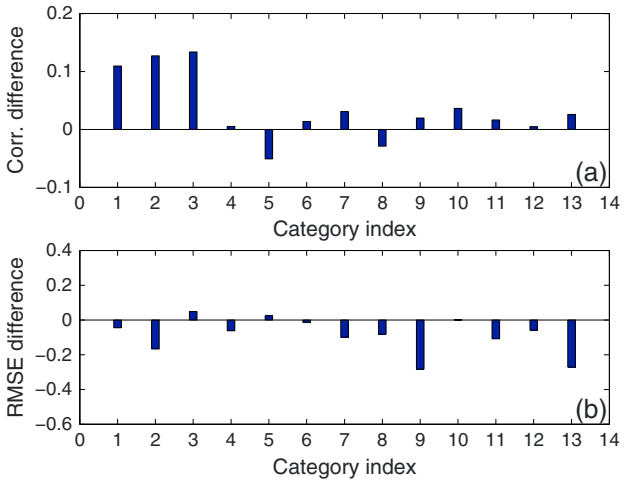

Figure 13. As in Figure 11 except for snowfall.

On the contrary, in category 3 the rain rate-TB relation in the stratified database is quite different from that in the validation data set. Instead, the regression curve between rain rate and TBs in the validation data set are more similar to that from the single database. Under this scenario, the single database will produce better retrieval results.

A similar procedure is applied to snowfall retrieval results. Figure 13 shows that over vast majority of the categories (92% for correlation and 89% for rmse) the correlation coefficient is larger and the rmse is smaller for the result from stratified databases. The underlying reason for this phenomenon is similar to that in the rainfall retrieval case studies (Figures 12 and 14). That is, whether

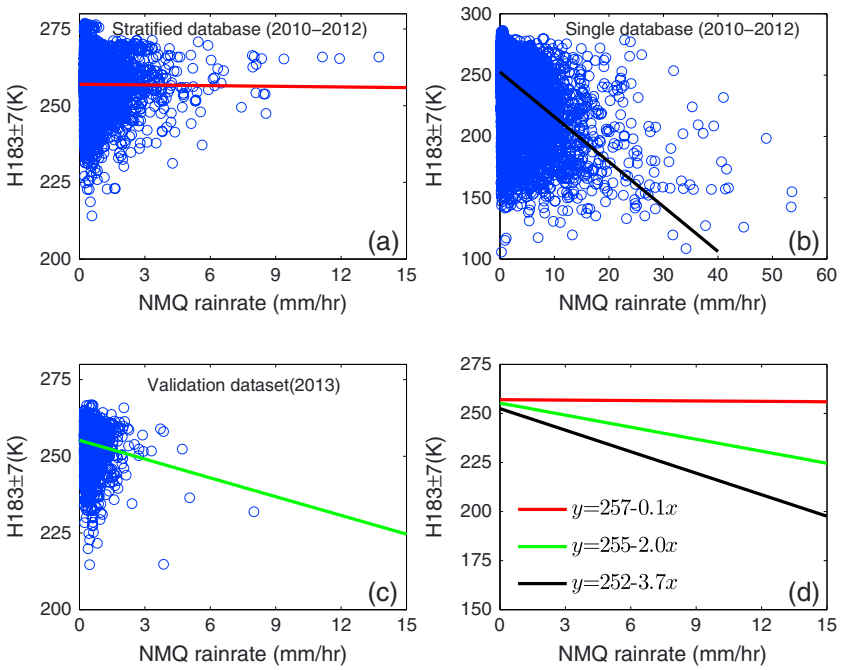

Figure 14. As in Figure 12 except for the category in which the better result is from the single database.

the better performance is from the single database or from stratified databases depends on the snow rate-TB relation in the validation data set if closer to that in the single database or to that in the corresponding stratified database.

To summarize, over the majority of the categories, the rain rate-TB at H183 ± 7 relations in the validation data sets are more similar to that in the stratified databases; therefore, overall, better performances are achieved when stratified databases are utilized.

6. Conclusions and Discussions

In this study, we utilized 4 year NMQ and SSMIS coincident databases to develop a prototype precipitation retrieval algorithm. Three year data (from 2010 to 2012) are taken as training data sets, while 1 year data (2013) are taken as a validation data set. The primary objective of this study was to explore the benefits of using ancillary data to stratify the single database into many smaller but more homogeneous databases. A requirement in our methodology is to make sure the surface condition and precipitation vertical structure are as similar as possible for both detection and precipitation rate retrieval processes. Four variables (surface type, surface temperature, land elevation, and ice layer thickness) are used to stratify the single database into dozens of smaller databases of similar surface condition and precipitation vertical structures. The performance using the stratified databases are compared with that using the single database.

The LDA technique is employed for the precipitation detection. For rainfall detection, compared with that using the single database, the POD using stratified databases increases from 75.9% to 84.0%, corresponding to a FAR of 0.05. On the other hand, corresponding to the same FAR, the POD for snowfall detection increases about 12% from 56.0% to 68.0% using stratified databases. In addition, it was found that by including lower troposphere relative humidity and vertical velocity at 700 hPa (besides the TBs), the POD for snow detection further increases to 76.4%, which is 20.4% higher than that only using TBs in the single database. However, including relative humidity and vertical velocity does not have significant influence for the rainfall detection. It is hypothesized that snowfall occurrence is more sensitive to the large-scale atmospheric backgrounds than rainfall because it is primarily a stratiform process. We are aware that the only the clear-sky radiances (i.e., TBs) are used in the process of data assimilation for MERRA data. More importantly, the relative humidity and vertical velocity are purely generated from models. Therefore, the better detection performance by adding relative humidity and vertical velocity is not due to a circular usage of the same TBs.

The PCA-based Bayesian technique is used to retrieve the precipitation rate after the detection. Compared with that from the single database, the retrieved rain rate using stratified databases agrees better with observations, indicated by larger Heidke Skill Score (HSS) in both ends of the rain rates. In particular, there is almost no skill when using the single database for rain rate larger than 30 mm/h. In contrast, using stratified databases will generate some skill for heavy rainfall. For the retrieved snow rate, larger HSS is evident throughout the snowfall range when the stratified databases are utilized.

The correlation coefficient between retrieved rain rates from stratified databases and observations is 0.63, while it is 0.42 for the rain rates retrieved from the single database. The root-mean-square error is reduced by about 53.2% from 2.03 to 0.98. The performance of the retrieved rain rate from the single database and stratified databases has also been investigated in the four seasons of 2013. It is found that from spring to fall the retrieved rain rates using stratified databases are better correlated with observations and the rmse is smaller. In the winter season, the retrieved results from the single database and stratified databases are comparable, although the underestimation of the retrieved rain rates from the single database is more severe. For snowfall, noticeable improvements have also been observed when stratified databases are employed. Additionally, due to the smaller dynamic range of the precipitation rate in the winter season, it is less likely to produce retrieved precipitation rates dramatically further apart from observations since the Bayesian algorithm seeks the optimal weighted average from the historical databases. This is supported by our results which show only marginal improvement in the winter season. For our study period the spatial pattern of the rain rate retrieved using stratified databases agrees better with NMQ observations. There is systematic overestimation over western United States for the retrieved rain rate from the single database. This overestimation is largely mitigated when stratified databases are employed.

Furthermore, we also analyzed the underlying reason that using stratified databases generally provides superior retrieved precipitation results. In essence, performance of the retrieved precipitation rate depends on whether the TB-precipitation rate in the validate data set is more similar to that in the single database or that in the corresponding stratified database. It is found that over the majority of the categories the TB-precipitation rate relations in each category in the validation data set are much closer to that in the corresponding stratified database. Therefore, over the majority of categories the retrieved precipitation rate from stratified databases are better correlated with observations and the rmse is smaller. Thus, overall, better performance is achieved by using stratified databases. Indeed, there exist some categories, the relation between TB and precipitation in the training stratified databases differ from those in the validation data sets, and rather the relation is more similar to that derived from the single database. With more data being collected, the historical data in each category will become more representative. Therefore, it is expected the retrieved results from stratified databases will outperform that from the single database.

This prototype algorithm has the potential to be applied in the global scale. It is highly likely that the databases generated over the continental United States ground radar observations may not be representative enough for all precipitation systems around the world, especially for the cloud systems over the tropical and higher-latitude regions. Along with the successful launch of GPM satellite, which carries both Ka- and Ku-band precipitation radars and has a quasi-global coverage, the representative issue can be largely alleviated.

We are aware that there exist biases in the NMQ precipitation products. It is not our purpose to define the precipitation climatology over the targeted region (25° – 50°N, 70° – 130°W) using NMQ data. Instead, we attempt to construct a common database from NMQ data to demonstrate that using stratified databases will significantly improve the precipitation retrieval result. In the near future, it may be possible to construct a database over more diverse climate regimes using observations from dual-frequency precipitation radar on the GPM satellite.

In addition, how to obtain the boundary values for each selected parameters is also of critical importance for the algorithm performance. For example, in this work, we simply divided the surface temperature into three subcategories by using the thresholds corresponding to the 33.3% and 66.7% of the surface temperature. These boundary values are probably not the optimal ones. How to find the optimal boundary values remains a challenging issue, and we are currently investigating this problem.

Finally, it is worth mentioning that the most current Goddard profiling algorithm (GPROF2014) has moved toward using other information to stratify the single database. The three parameters used in GPROF2014 are surface type, surface skin temperature, and total precipitable water. On the other hand, the parameters used in

this work are surface type, surface skin temperature, land elevation, and ice layer thickness. Which parameters can more effectively capture both the cloud vertical structure and surface condition information remains to be answered. In fact, which ancillary parameters can most effectively stratify the single database and therefore alleviate the ill-posed inversion problem is probably the most important issue to be considered in the passive microwave precipitation retrieval algorithm development.

Acknowledgments

NMQ data were provided by J. J. Gourley and Pierre Kirstetter of the National Severe Storms Laboratory (NSSL) of NOAA at Oklahoma (http://www.nssl.noaa.gov/contact.php). SSMIS data were provided by Colorado State University courtesy of Wesley Berg (berg@atmos.colostate.edu). The authors thank Jun Dong at ESSIC for assistance in processing the NMQ data. We also thank the constructive comments from Kazumasa Aonashi and two other anonymous reviewers. This research is supported by NOAA grant NA09NES4400006.

References

Adler, R. F., A. J. Negri, P. R. Keehn, and I. M. Hakkarinen (1993), Estimation of monthly rainfall over Japan and surrounding waters from a combination of low-orbit microwave and geosynchronous IR data, *J. Appl. Meteorol.*, *32*(2), 335–356.

Adler, R. F., G. J. Huffman, and P. R. Keehn (1994), Global tropical rain estimates from microwave-adjusted geosynchronous IR data, *Remote Sens. Rev.*, *11*(1-4), 125–152.

Aires, F., C. Prigent, F. Bernardo, C. Jiménez, R. Saunders, and P. Brunel (2011), A tool to estimate land-surface emissivities at microwave frequencies (TELSEM) for use in numerical weather prediction, *Q. J. R. Meteorol. Soc.*, *137*(656), 690–699.

Aonashi, K., et al. (2009), GSMaP passive microwave precipitation retrieval algorithm: Algorithm description and validation, *J. Meteorol. Soc. Jpn.*, *87*, 119–136.

Austin, R. T., A. J. Heymsfield, and G. L. Stephens (2009), Retrieval of ice cloud microphysical parameters using the CloudSat millimeter-wave radar and temperature, *J. Geophys. Res.*, *114*, D00A23, doi:10.1029/2008JD010049.

Bauer, P., and R. Bennartz (1998), Tropical rainfall measuring mission microwave imaging capabilities for the observation of rain clouds, *Radio Sci.*, *33*(2), 335–349.

Bennartz, R., and P. Bauer (2003), Sensitivity of microwave radiances at 85–183 GHz to precipitating ice particles, *Radio Sci.*, *38*(4), 8075, doi:10.1029/2002RS002626.

Berg, W., C. Kummerow, and C. Morales (2002), Differences between east and west Pacific rainfall systems, *J. Clim.*, *15*(24), 3659–3672.

Chen, S., J. J. Gourley, Y. Hong, P. Kirstetter, J. Zhang, K. Howard, Z. L. Flamig, J. Hu, and Y. Qi (2013), Evaluation and uncertainty estimation of NOAA/NSSL next-generation National Mosaic Quantitative Precipitation Estimation product (Q2) over the continental United States, *J. Hydrometeorol.*, *14*, 1308–1322.

Chiu, J. C., and G. W. Petty (2006), Bayesian retrieval of complete posterior PDFs of oceanic rain rate from microwave observations, *J. Appl. Meteorol. Climatol.*, *45*(8), 1073–1095.

Conner, M. D., and G. W. Petty (1998), Validation and intercomparison of SSM/I rain-rate retrieval methods over the continental United States, *J. Appl. Meteorol.*, *37*(7), 679–700.

Evans, K., et al. (2012), Ice hydrometeor profile retrieval algorithm for high frequency microwave radiometers: Application to the CoSSIR instrument during TC4, *Atmos. Meas. Tech. Discuss.*, *5*(2), 3117–3198.

Evans, K. F., J. Turk, T. Wong, and G. L. Stephens (1995), A Bayesian approach to microwave precipitation profile retrieval, *J. Appl. Meteorol.*, *34*(1), 260–279.

Evans, K. F., S. J. Walter, A. J. Heymsfield, and G. M. McFarquhar (2002), Submillimeter-wave cloud ice radiometer: Simulations of retrieval algorithm performance, *J. Geophys. Res.*, *107*(D3), 4028, doi:10.1029/2001JD000709.

Farrar, M. R., and E. A. Smith (1992), Spatial resolution enhancement of terrestrial features using deconvolved SSM/I microwave brightness temperatures, *IEEE Trans. Geosci. Remote Sens.*, *30*(2), 349–355.

Ferraro, R. R., and G. F. Marks (1995), The development of ssm/i rain-rate retrieval algorithms using ground-based radar measurements, *J. Atmos. Oceanic Technol.*, *12*(4), 755–770.

Ferraro, R. R., N. C. Grody, and G. F. Marks (1994), Effects of surface conditions on rain identification using the DMSP-SSM/I, *Remote Sens. Rev.*, *11*(1-4), 195–209.

Ferraro, R. R., et al. (2013), An evaluation of microwave land surface emissivities over the continental United States to benefit GPM-era precipitation algorithms, *IEEE Trans. Geosci. Remote Sens.*, *51*(1), 378–398.

Gebregiorgis, A. S., and F. Hossain (2013), Understanding the dependence of satellite rainfall uncertainty on topography and climate for hydrologic model simulation, *IEEE Trans. Geosci. Remote Sens.*, *51*, 704–718.

Gopalan, K., N.-Y. Wang, R. Ferraro, and C. Liu (2010), Status of the TRMM 2A12 land precipitation algorithm, *J. Atmos. Oceanic Technol.*, *27*(8), 1343–1354.

Grody, N. C. (1991), Classification of snow cover and precipitation using the special sensor microwave imager, *J. Geophys. Res.*, *96*(D4), 7423–7435.

Harris, G., K. Bowman, and D. Shin (2000), Comparison of freezing-level altitudes from the NCEP reanalysis with TRMM precipitation radar brightband data, *J. Clim.*, *13*(23), 4137–4148.

Hastings, D. A., and P. Dunbar (1998), Development & assessment of the Global Land One-km Base Elevation digital elevation model (GLOBE), *Int. Arch. Photogramm. Remote Sens.*, *32*(4), 218–221.

Hirose, M., and K. Nakamura (2004), Spatiotemporal variation of the vertical gradient of rainfall rate observed by the TRMM precipitation radar, *J. Clim.*, *17*, 3378–3397.

Kacimi, S., N. Viltard, and P.-E. Kirstetter (2013), A new methodology for rain identification from passive microwave data in the tropics using neural networks, *Q. J. R. Meteorol. Soc.*, *139*, 912–922, doi:10.1002/qj.2114.

Katsumata, M., H. Uyeda, K. Iwanami, and G. Liu (2000), The response of 36- and 89-GHz microwave channels to convective snow clouds over ocean: Observation and modeling, *J. Appl. Meteorol.*, *39*(12), 2322–2335.

Kim, M.-J., J. Weinman, W. Olson, D.-E. Chang, G. Skofronick-Jackson, and J. Wang (2008), A physical model to estimate snowfall over land using AMSU-B observations, *J. Geophys. Res.*, *113*, D09201, doi:10.1029/2007JD008589.

Kongoli, C., P. Pellegrino, R. R. Ferraro, N. C. Grody, and H. Meng (2003), A new snowfall detection algorithm over land using measurements from the Advanced Microwave Sounding Unit (AMSU), *Geophys. Res. Lett.*, *30*(14), 1756, doi:10.1029/2003GL017177.

Kummerow, C., W. S. Olson, and L. Giglio (1996), A simplified scheme for obtaining precipitation and vertical hydrometeor profiles from passive microwave sensors, *IEEE Trans. Geosci. Remote Sens.*, *34*(5), 1213–1232.

Kummerow, C. D., S. Ringerud, J. Crook, D. Randel, and W. Berg (2011), An observationally generated a priori database for microwave rainfall retrievals, *J. Atmos. Oceanic Technol.*, *28*(2), 113–130.

L'ecuyer, T. S., and G. L. Stephens (2002), An uncertainty model for Bayesian Monte Carlo retrieval algorithms: Application to the TRMM observing system, *Q. J. R. Meteorol. Soc.*, *128*(583), 1713–1737.

Lin, X., and A. Y. Hou (2008), Evaluation of coincident passive microwave rainfall estimates using TRMM PR and ground measurements as references, *J. Appl. Meteorol. Climatol.*, *47*(12), 3170–3187.

Liu, C., and E. J. Zipser (2013), Why does radar reflectivity tend to increase downward toward the ocean surface, but decrease downward toward the land surface?, *J. Geophys. Res. Atmos.*, *118*, 135–148, doi:10.1029/2012JD018134.
Liu, G. (2008), Deriving snow cloud characteristics from CloudSat observations, *J. Geophys. Res.*, *113*, D00A09, doi:10.1029/2007JD009766.
Liu, G., and J. A. Curry (1992), Retrieval of precipitation from satellite microwave measurement using both emission and scattering, *J. Geophys. Res.*, *97*(D9), 9959–9974.
Liu, G., and Y. Fu (2001), The characteristics of tropical precipitation profiles as inferred from satellite radar measurements, *J. Meteorol. Soc. Jpn.*, *79*(1), 131–143.
Liu, G., and E.-K. Seo (2013), Detecting snowfall over land by satellite high-frequency microwave observations: The lack of scattering signature and a statistical approach, *J. Geophys. Res. Atmos.*, *118*, 1376–1387, doi:10.1002/jgrd.50172.
Lorenc, A. C. (1986), Analysis methods for numerical weather prediction, *Q. J. R. Meteorol. Soc.*, *112*(474), 1177–1194.
McCollum, J. R., and R. R. Ferraro (2003), Next generation of NOAA/NESDIS TMI, SSM/I, and AMSR-E microwave land rainfall algorithms, *J. Geophys. Res.*, *108*(D8), 8382, doi:10.1029/2001JD001512.
Munchak, S. J., and G. Skofronick-Jackson (2013), Evaluation of precipitation detection over various surfaces from passive microwave imagers and sounders, *Atmos. Res.*, *131*, 81–94.
Noh, Y.-J., G. Liu, E.-K. Seo, J. R. Wang, and K. Aonashi (2006), Development of a snowfall retrieval algorithm at high microwave frequencies, *J. Geophys. Res.*, *111*, D22216, doi:10.1029/2005JD006826.
Petty, G. W., and K. Li (2013), Improved passive microwave retrievals of rain rate over land and ocean. Part II: Validation and intercomparison, *J. Atmos. Oceanic Technol.*, *30*, 2509–2526.
Prigent, C., F. Aires, and W. Rossow (2006), Land surface microwave emissivities over the globe for a decade, *Bull. Am. Meteorol. Soc.*, *87*(11), 1573–1584.
Rapp, A. D., M. Lebsock, and C. Kummerow (2009), On the consequences of resampling microwave radiometer observations for use in retrieval algorithms, *J. Appl. Meteorol. Climatol.*, *48*(9), 1981–1993.
Rienecker, M. M., et al. (2011), MERRA: NASA's modern-era retrospective analysis for research and applications, *J. Clim.*, *24*(14), 3624–3648.
Rodgers, C. D. (1976), Retrieval of atmospheric temperature and composition from remote measurements of thermal radiation, *Rev. Geophys.*, *14*(4), 609–624.
Sano, P., D. Casella, A. Mugnai, G. Schiavon, E. A. Smith, and G. J. Tripoli (2013), Transitioning from CRD to CDRD in Bayesian retrieval of rainfall from satellite passive microwave measurements: Part 1. Algorithm description and testing, *IEEE Trans. Geosci. Remote Sens.*, *51*(7), 4119–4143.
Seto, S., N. Takahashi, and T. Iguchi (2005), Rain/no-rain classification methods for microwave radiometer observations over land using statistical information for brightness temperatures under no-rain conditions, *J. Appl. Meteorol.*, *44*(8), 1243–1259.
Skofronick-Jackson, G. M., M.-J. Kim, J. A. Weinman, and D.-E. Chang (2004), A physical model to determine snowfall over land by microwave radiometry, *IEEE Trans. Geosci. Remote Sens.*, *42*(5), 1047–1058.
Skofronick-Jackson, G. M., B. T. Johnson, and S. J. Munchak (2013), Detection thresholds of falling snow from satellite-borne active and passive sensors, *IEEE Trans. Geosci. Remote Sens.*, *51*, 4177–4189.
Smith, E., H. Leung, J. Elsner, A. Mehta, G. Tripoli, D. Casella, S. Dietrich, A. Mugnai, G. Panegrossi, and P. Sanò (2013), Transitioning from CRD to CDRD in Bayesian retrieval of rainfall from satellite passive microwave measurements: Part 3—Identification of optimal meteorological tags, *Nat. Hazard. Earth Syst. Sci*, *13*, 1185–1208.
Spencer, R. W., H. M. Goodman, and R. E. Hood (1989), Precipitation retrieval over land and ocean with the SSM/I: Identification and characteristics of the scattering signal, *J. Atmos. Oceanic Technol.*, *6*(2), 254–273.
Staelin, D. H., and F. W. Chen (2000), Precipitation observations near 54 and 183 GHz using the NOAA-15 satellite, *IEEE Trans. Geosci. Remote Sens.*, *38*(5), 2322–2332.
Tang, L., Y. Tian, and X. Lin (2014), Validation of precipitation retrievals over land from satellite-based passive microwave sensors, *J. Geophys. Res. Atmos.*, *119*, 4546–4567, doi:10.1002/2013JD020933.
Turk, F. J., Z. S. Haddad, and Y. You (2013), Principal components of multi-frequency microwave land surface emissivities. Part 1: Estimation under clear and precipitating conditions, *J. Hydrometeorol.*, *15*, 3–19.
Viltard, N., C. Burlaud, and C. D. Kummerow (2006), Rain retrieval from TMI brightness temperature measurements using a TRMM PR-based database, *J. Appl. Meteorol. Climatol.*, *45*(3), 455–466.
Wang, N.-Y., C. Liu, R. Ferraro, D. Wolff, E. Zipser, and C. Kummerow (2009), TRMM 2A12 land precipitation product—Status and future plans, *J. Meteorol. Soc. Jpn. A*, *87*, 237–253.
Wang, N.-Y., K. Gopalan, and R. I. Albrecht (2012), Application of lightning to passive microwave convective and stratiform partitioning in passive microwave rainfall retrieval algorithm over land from TRMM, *J. Geophys. Res.*, *117*, D23203, doi:10.1029/2012JD017812.
Wilks, D. S. (2011), *Statistical Methods in the Atmospheric Sciences*, vol. 100, Elsevier, Ithaca, N. Y.
Yan, B., and F. Weng (2008), Intercalibration between special sensor microwave imager/sounder and special sensor microwave imager, *IEEE Trans. Geosci. Remote Sens.*, *46*(4), 984–995.
You, Y. (2013), A new over-land rainfall retrieval algorithm using satellite microwave observations, PhD thesis, The Florida State Univ., Tallahassee.
You, Y., and G. Liu (2012), The relationship between surface rainrate and water paths and its implications to satellite rainrate retrieval, *J. Geophys. Res.*, *117*, D13207, doi:10.1029/2012JD017662.
You, Y., G. Liu, Y. Wang, and J. Cao (2011), On the sensitivity of Tropical Rainfall Measuring Mission (TRMM) microwave imager channels to overland rainfall, *J. Geophys. Res.*, *116*, D12203, doi:10.1029/2010JD015345.
You, Y., F. J. Turk, Z. S. Haddad, L. Li, and G. Liu (2013), Principal components of multi-frequency microwave land surface emissivities. Part 2: Effects of previous-time precipitation, *J. Hydrometeorol.*, *15*, 20–37.
Zhang, J., et al. (2011), National Mosaic and Multi-Sensor QPE (NMQ) system: Description, results, and future plans, *Bull. Am. Meteorol. Soc.*, *92*(10), 1321–1338.
Zipser, E. J., C. Liu, D. J. Cecil, S. W. Nesbitt, and D. P. Yorty (2006), Where are the most intense thunderstorms on Earth?, *Bull. Am. Meteorol. Soc.*, *87*(8), 1057–1071.